Exp Fluids (2008) 44:951–959
DOI 10.1007/s00348-007-0454-4

RESEARCH ARTICLE

Measurement of velocity profiles in a rectangular microchannel with aspect ratio $\alpha = 0.35$

Xu Zheng · Zhan-hua Silber-Li

Received: 30 October 2006 / Revised: 25 November 2007 / Accepted: 12 December 2007 / Published online: 24 January 2008

Abstract In this work, we measured 14 horizontal velocity profiles along the vertical direction of a rectangular microchannel with aspect ratio $\alpha = h/w = 0.35$ (h is the height of the channel and w is the width of the channel) using microPIV at $Re = 1.8$ and 3.6. The experimental velocity profiles are compared with the full 3D theoretical solution, and also with a Poiseuille parabolic profile. It is shown that the experimental velocity profiles in the horizontal and vertical planes are in agreement with the theoretical profiles, except for the planes close to the wall. The discrepancies between the experimental data and 3D theoretical results in the center vertical plane are less than 3.6%. But the deviations between experimental data and Poiseuille's results approaches 5%. It indicates that 2D Poiseuille profile is no longer a perfect theoretical approximation since $\alpha = 0.35$. The experiments also reveal that, very near the hydrophilic wall ($z = 0.5$–1 μm), the measured velocities are significantly larger than the theoretical velocity based on the no-slip assumption. A proper discussion on some physical effects influencing the near wall velocity measurement is given.

1 Introduction

The cross-sections of microchannels in microfluidic chips are often rectangular, and clearly a detailed understanding of velocity profiles is important for chip design and capability analysis.

There are plenty of studies about velocity profiles in macro-scale flows. Boussinesq (1868), and then White (1974) presented the exact solution of the velocity profile in a rectangular channel by solving the Navier–Stokes (N–S) equations with the no-slip boundary condition at the wall. Patel and Head (1969) gave the distributions of the maximum velocities in different horizontal planes in rectangular channels, at different Re numbers. Schlichting (1979) summarized the results of Nikuradse's experiments, and presented a series of iso-velocity curves in a rectangular pipe.

For micro-scale flows, velocity profiles of transition flow in rectangular channels ($Re = 200$–$2{,}000$) were studied systematically (Li and Olsen 2006). But for low Re, there are few studies of full-field velocity profiles. Several studies have given the velocity profile in a certain plane or part of the channel. For instance, Tretheway and Meinhart (2002) used a microPIV system to measure the velocity profiles at $z^+ = 0.5$ ($z^+ = z/h$, with the coordinates as shown in Fig. 1) in a rectangular microchannel (the height $h = 30$ μm, the width $w = 300$ μm, $\alpha = h/w = 0.1$), to study the slip at the hydrophobic/hydrophilic side wall. Devasenathipathy et al. (2003) also measured the velocity profile at the central plane $z^+ = 0.5$ upon glass substrate in a rectangular microchannel ($h = 107$ μm, $w = 100$ μm, $\alpha = 1.07$) fabricated out of a single-crystal silicon wafer. The measured velocities are consistent with the expected theoretical values. Joseph and Tabeling (2005) studied the slip on the walls of a poly-dimethylsiloxane (PDMS) rectangular microchannel on a glass substrate ($h = 10$ μm, $w = 100$ μm, $\alpha = 0.1$). They used a parabolic profile to fit the experimental data measured in the central vertical plane (x-o-z plane). Ou and Rothstein (2005) measured the

X. Zheng · Z. Silber-Li (✉)
LNM, Institute of Mechanics, Chinese Academy of Sciences, 100080 Beijing, China
e-mail: lili@imech.ac.cn

X. Zheng
e-mail: zhengxu@lnm.imech.ac.cn

velocities in several rectangular microchannels with h = 76–254 μm and fixed α = 0.05. The super-hydrophobic substrate wall of the channels consisted of micro-ridges, and large velocity increases near this wall were observed. In these references mentioned above, the aspect ratios of the microchannels are $\alpha \leq 0.1$ or $\alpha \approx 1.0$. But for flow in microchannels, the measurement of the velocity profiles in the whole flow field with moderate aspect ratio is lacking. Generally, the theoretical velocity profile of flows through a channel of rectangular cross-section is given by a series solution of the N–S equation, and Poiseuille parabolic profile is used as an approximate profile in rectangular cross-section with small aspect ratio, i.e. $\alpha \leq 0.1$. Stone et al. (2004) suggested that the difference between theoretical velocity profile and 2D Poiseuille profile is larger than 10% for a rectangular channel with α = 0.7. So it is worthwhile measuring the detailed velocity profile in a rectangular microchannel with moderate aspect ratio α.

Using the coordinates as shown in Fig. 1, the theoretical velocity solution of the N–S equation with a no-slip boundary condition is expressed as (e.g. White 1974):

$$u_x(y,z) = \frac{4h^2\Delta p}{\pi^3\mu L}\sum_{n=1,3,5\ldots}^{\infty}\frac{1}{n^3}\left[1-\frac{\cosh(n\pi\frac{y}{h})}{\cosh(n\pi\frac{w}{2h})}\right]\sin\left(n\pi\frac{z}{h}\right) \tag{1}$$

The flow rate can be obtained by integrating Eq. 1:

$$\begin{aligned} Q &= 2\int_0^{\frac{1}{2}w}\int_0^{h} u_x \mathrm{d}y\mathrm{d}z \\ &= \frac{wh^3\Delta p}{12\mu L}\left[1-\sum_{n=1,3,5\ldots}^{\infty}\frac{1}{n^5}\frac{192}{\pi^5}\frac{h}{w}\tanh\left(n\pi\frac{w}{2h}\right)\right] \\ &= Q_P\left[1-\sum_{n=1,3,5\ldots}^{\infty}\frac{1}{n^5}\frac{192}{\pi^5}\alpha\tanh\left(\frac{n\pi}{2\alpha}\right)\right] \end{aligned} \tag{2}$$

where L, w and h are the length, width and height of the channel, respectively, Δp is the driven pressure drop, μ is the viscosity of liquid, Q_P is the flow rate calculated from the formula of 2D Poiseuille flow. It is shown clearly that u_x and Q are smaller than those obtained from Poiseuille model, due to the terms with minus sign in the series in Eqs. 1 and 2. When $n = 5$ is chosen as the cut off value in Eq. 1, the error of the high order terms is approximately 0.43%. The discrepancy between the theoretical value and Poiseuille's value will increase with the increase of the aspect ratio. For a rectangular channel with α = 0.35, the discrepancy of mean velocity can approach 5% when $n \leq 5$.

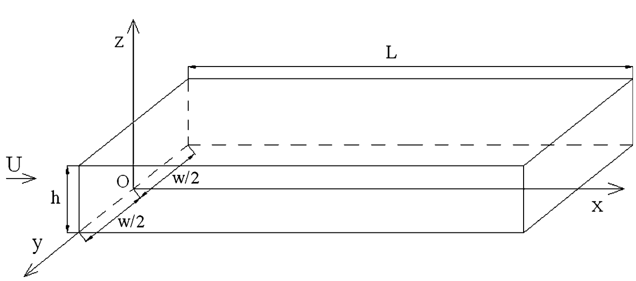

Fig. 1 Schematic diagram of the rectangular microchannel and the coordinate system, the width of the channel is w (y direction), the height of the channel is h (z direction)

In this paper, we will study the detailed velocity profiles in a rectangular microchannel (h = 19.1 μm, w = 54 μm, α = 0.35) using microPIV system, from z^+ = 0.026 to 0.94. Section 2 will describe the microPIV system and the measuring method. In Sect. 3 the experimental velocity profiles will be presented and compared with theoretical profile and Poiseuille profile. Then a proper discussion is given to analyze the velocity measurement very near wall in Sect. 4. The conclusions of the paper will be given at the end.

2 Experimental apparatus and methods

2.1 Experimental apparatus

The flow field measurement is carried out by a microflow measuring system of the LNM, Institute of Mechanics, CAS. It includes a microPIV system and a pressure driven flow system. The microPIV system (Fig. 2) is mainly composed of a double pulsed Nd:YAG laser (New Wave 120XT, 532 nm), a fluorescent inverted microscope (Olympus IX71), an EMCCD (Andor DV885), a nano-scale vertical adjustment instrument with a piezo-transducer

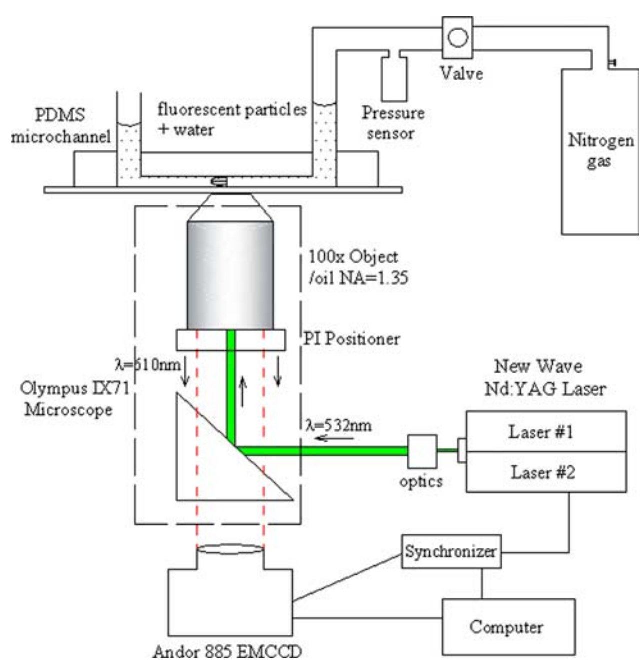

Fig. 2 Schematic diagram of experimental set-up

(Physik Instrument LVPZT E665) and a synchronization controller (Lifangtiandi micropulse 710). The flow is pressure driven in conjunction with a high pressure nitrogen gas tank, a pressure transducer and a temperature transducer (Silber-Li et al. 2004).

2.2 Specifications of microPIV

1. Laser: the double pulsed Nd:YAG laser operates at 532 nm, it can emit two pulses with an adjustable time interval Δt = 100 ns–1 s controlled by a synchronization controller, at a frequency from 1 to 15 Hz. The power of the pulsed laser used in the experiments was 10–15 mJ.
2. Objective: a 100× oil immersed objective is chosen, with the numerical aperture NA = 1.35. The refractive index n_r of the objective oil is 1.516. The optical resolution can be evaluated as $\delta \approx 0.28$ μm according to the formula of the optical resolution limit. The working distance WD of the objective is approximately 100 μm. WD is defined as the distance between the objective front lens and the focus plane.
3. Fluorescent particles: the fluorescent polystyrene particles (Duke Scientific Corporation) are used as tracers in the experiments. The mean diameter d_p of the particles is 200 nm, and the density is approximately 1.05 g/cm^3, close to that of water. The volume concentration of the fluorescent particles was diluted to approximately 0.01% in the experiment. The fluorescent particle diameters of diffractive-limited point-spread function d_s and the effective particle diameter d_e can be calculated as (Meinhart et al. 1999):

$$d_s = 1.22M\frac{\lambda}{NA} \tag{3}$$

$$d_e = \sqrt{M^2 d_p^2 + d_s^2} \tag{4}$$

where M is the magnification of the objective, λ is the wave length of the emission light, and the NA is the numerical aperture. In our experiments, M = 100, $\lambda \approx 610$ nm, NA = 1.35, as a result, d_s = 55.1 μm and d_e = 58.6 μm. When the magnification M = 100, the effective diameter of the particle spot is d_e/M = 586 nm.

The influence of Brownian motion must be considered for submicron particles. A first order estimation of error due to Brownian motion ε_B is given by Santiago et al. (1998) is expressed as:

$$\varepsilon_B = \frac{1}{u}\sqrt{\frac{2D}{\Delta t}} \tag{5}$$

Here, u is the characteristic velocity, Δt is the time interval between the two pulses of laser and D the diffusion coefficient. The values of the diffusion coefficient are calculated with the method given by Lauga and Squires (2005). Based on different values of u and Δt, the errors ε_B due to Brownian motion are calculated in Table 1. The results show that the Brownian motion error is less than 1%, and will thus be neglected.

Table 1 Errors due to Brownian motion

	Position (μm)	u (m/s)	D (m^2/s)	Δt (μs)	Error ε_B (%)
Exp. 1 Re = 1.8	z = 0.5	0.006	2.04×10^{-12}	1,000	1
	z = 8–10	0.052	2.29×10^{-12}	30	0.75
Exp. 2 Re = 3.6	z = 0.5	0.012	2.04×10^{-12}	700	0.64
	z = 8–10	0.105	2.29×10^{-12}	20	0.46

4. CCD: a 1,004 × 1,002 pixels 14 bit EMCCD is used to capture images, with 35 MHz read out frequency. Its gain can be adjusted to improve signal-noise ratio. When the EMCCD works at a temperature below −70°C, the dark current is only 0.007e/(pix·s), and the quantum efficiency is 70%. The pixel size is 8 × 8 μm. With the fluorescent microscope, a digital image resolution of 80 nm can be reached under 1 × 1 binning model. During the experiment, the emission of two sequential laser pulses is controlled by the synchronization controller with the time interval Δt ranging from 20 μs (measurement position is at central area of the channel) to 1.0 ms (measurement position is near wall).

2.3 Fabrication of the rectangular microchannel

The rectangular microchannels in the experiments were fabricated using hydrophobic PDMS using MEMS classical soft-lithography technique. The channels then were bonded on the glass substrates using oxygenic ion sputtering. The contact angle (CA) on the glass substrate is 20–30°, and that on the PDMS wall is 95°. The geometric sizes of two microchannels used in experiments are shown in Table 2 with their measured accuracies. The image of the cross-section (Fig. 3) shows that the walls of the channel are perpendicular to each other, and the walls are

Table 2 The geometric sizes of the microchannels

Microchannel	Width w (μm)	Height h (μm)	Aspect ratio α	Length L (mm)
1	54.0 ± 0.1	19.1 ± 0.1	0.35	27.90 ± 0.02
2	54.0 ± 0.1	19.1 ± 0.1	0.35	26.62 ± 0.02

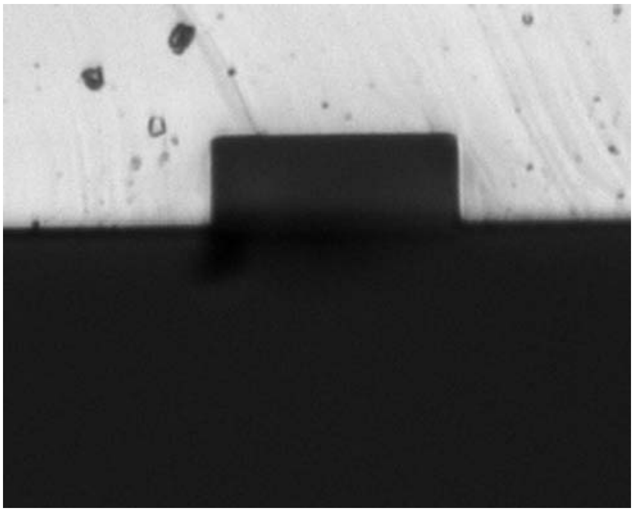

Fig. 3 A photograph of the cross-section of the rectangular microchannel

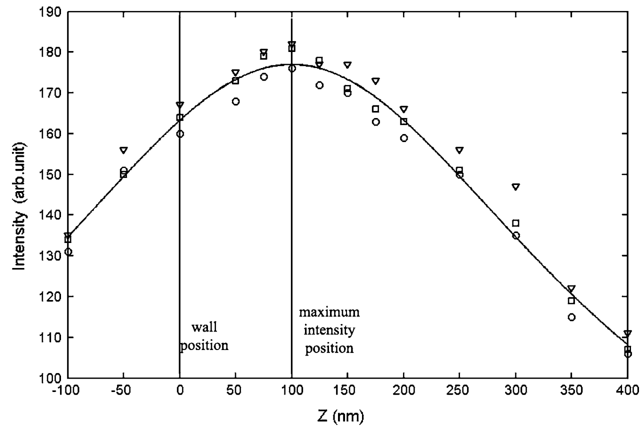

Fig. 4 The distribution of the intensity of particles adsorbed to the wall

smooth. The distance from the measurement position to the inlet of the channel is approximately 1cm, which is significantly larger than the inlet length, so the influence of inlet effect can be neglected.

2.4 Determination of the wall position

The experiment began from the position of the glass substrate, which was set as $z = 0$ µm. The objective focal plane was adjusted by a piezo-transducer. The vertical adjustment range is from 0 to 100 µm with an accuracy of 10 nm. The fluorescent particles adsorbed to the substrate are used to determine the wall position: the intensity of the particle recorded by the CCD varies as the location of the focal plane is changed. According to the functional relation (Lorentzian distribution) between the intensity of the particle spot and the distance from the particle to the focal plane given by Olsen and Adrian (2000), the wall position can be determined from the intensity change of the adsorbed particles. We observed several adsorbed particles, and measured their intensity distributions along vertical direction z (Fig. 4). When these particles reached their maximum intensity, the particle centers are just at the focal plane. So the real wall position should be the focal plane minus one particle radius ($\approx$100 nm). This method of determining the wall position is accurate to within 50 nm.

2.5 Experimental procedures

During the experiment, the flow in the rectangular microchannel was driven by nitrogen gas (Fig. 2), the driving pressure ranging from 10 to 50 kPa was read out by a pressure transducer, whose accuracy was 0.3%. The pipes were connected to the inlet and the outlet of the microchannel, the height difference of the fluorescent liquid columns in pipes between the two ends was also considered. The environment temperature was approximately 25°C during the experiment, and the accuracy of the temperature transducer was 0.1°C. The experiment was carried out when the flow field was stable, and one group of images were captured at each 0.5 µm distance ($z^+ \approx 0.026$) along z direction near the wall, and at each 1–2 µm distance ($z^+ \approx 0.05$–0.1) in the other part of the channel. A group of images at each vertical position included 50–200 frames. The position of focal plane at each vertical position was adjusted by the piezo-transducer.

2.6 Image processing

The image captured by an Andor 885 EMCCD is 1,004 × 1,002 pixels, corresponding to an approximately 80 × 80 µm visual field. The first step of image processing was to filter or reduce the noise and intensify the image of the particle spots. A Digital filter proposed by Gui et al. (2002) was used to reduce the high frequency random noise. Additionally, a threshold gray-scale value was chosen to filter out the out-of-plane particles. An image after the preprocessing is shown in Fig. 5. The EMCCD does not have the double-exposure function, we have to capture two spots of the same fluorescent particle exited by the double laser pulses in one image during every exposure time Δt_e. Therefore, auto-correlation is used to calculate the particle displacements and hence velocities. The interrogation area was 128 × 16 pixels with 50% overlapping in the near wall region, and 64 × 16 pixels without overlapping in other positions. So all the calculated results had a 64 pixels step in x direction. The corresponding spatial resolution of the velocity field in x–y plane was 5.12 × 1.28 µm. This meant

Fig. 5 One image of the series recorded by microPIV after pre-processing

42 velocity vectors could be obtained along the width direction y and seven columns in the streamwise x direction (Fig. 6). The concentration of the particles was low, so the velocity vectors in Fig. 6 were calculated from the ensemble average of 50–200 successive frames (200 frames in near wall region, 50–100 frames in other region). The velocity profile in this horizontal plane was then averaged from the seven columns. The standard deviation σ, defined as $\sigma_n = \sqrt{\frac{1}{7}\sum_{m=1}^{7}\left[\left(u_{\exp,n}\right)_m - u_{\exp,n}\right]^2}$, is used to indicate the precision of the experimental data from this average. Here, the subscript m (m = 1–7) represents the number of velocity vector columns in Fig. 6, n (n = 1–42) represents the number of velocity vectors in each column, $\left(u_{\exp,n}\right)_m$ is the measured velocity at the nth point of the mth column, $u_{\exp,n}$ is the average velocity at the nth point calculated from the seven columns. The standard deviations over the seven-columns ensemble average were 2–3% (those in the area near the wall were 3–10%).

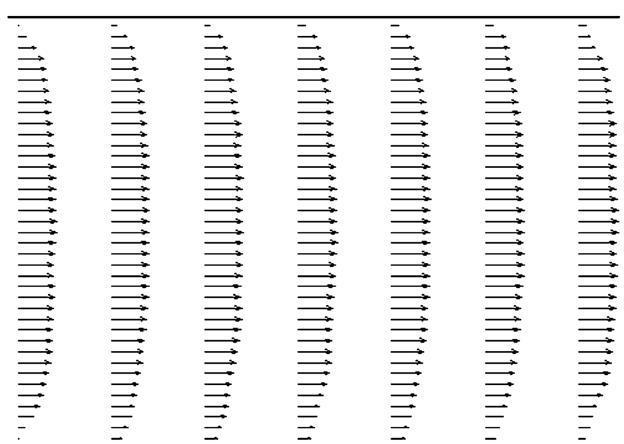

Fig. 6 The measured velocity vectors of the flow field in x–y plane

3 Experimental velocity profiles in rectangular microchannels

3.1 Theoretical velocity profile

A solution from no-slip N–S equation for a 3D geometric rectangular microchannel is used to describe the velocity profile (Eq. 1). An approximate theoretical expression is obtained when $n \leq 5$. The accuracy of Δp is 0.6%. The measurement accuracy of geometric sizes of the microchannel is given in Table 2. The error in the viscosity μ caused by the error in temperature measurement is 0.4%. So the uncertainty of the theoretical velocity calculated from the fifth order approximation of the theoretical equation Eq. 1 can be estimated to be approximately 1.3%, and the uncertainty of the theoretical flow rate calculated from Eq. 2 is approximately 1.7%. Furthermore, for the velocity in x–o–z plane, a 2D Poiseuille parabolic profile is also used to compare with the experimental results.

3.2 Experimental results

3.2.1 *Velocity profiles in* x–y *horizontal plane*

The experimental velocity profiles in 14 different x–y planes at $Re = 1.8$. Here, experimental data in 12 planes are shown in Fig. 7, and compared with the theoretical results. The relative deviation of the velocity value between the experimental data and the theoretical value for one point is defined as $\varepsilon_n = \frac{\left(u_{\exp,n} - u_{\mathrm{theo},n}\right)}{u_{\mathrm{theo},n}}$. To illustrate the discrepancy in a horizontal plane, the average relative deviation defined as $\bar{\varepsilon} = \frac{1}{42}\sum_{n=1}^{42}\frac{\left(u_{\exp,n} - u_{\mathrm{theo},n}\right)}{u_{\mathrm{theo},n}}$ is used. For clarity, the error bars for each data point based on the standard deviations σ are only marked in Fig. 7a.

In the near wall region (Fig. 7a, b), the experimental velocity profiles in the middle are relatively flat, which is the characteristic of velocity profiles in 3D flows through a channel of rectangular cross-section. The trends of experimental data are consistent with the theoretical profiles, but obviously, the experimental values are larger. At the positions of z = 0.5, 1.0, 1.5 and 2.0 μm ($z^+ = 0.026$–0.105), the average relative deviations $\bar{\varepsilon}$ are 10.2, 9.9, 3.8 and 2.3%, respectively, and at the center of each x–y

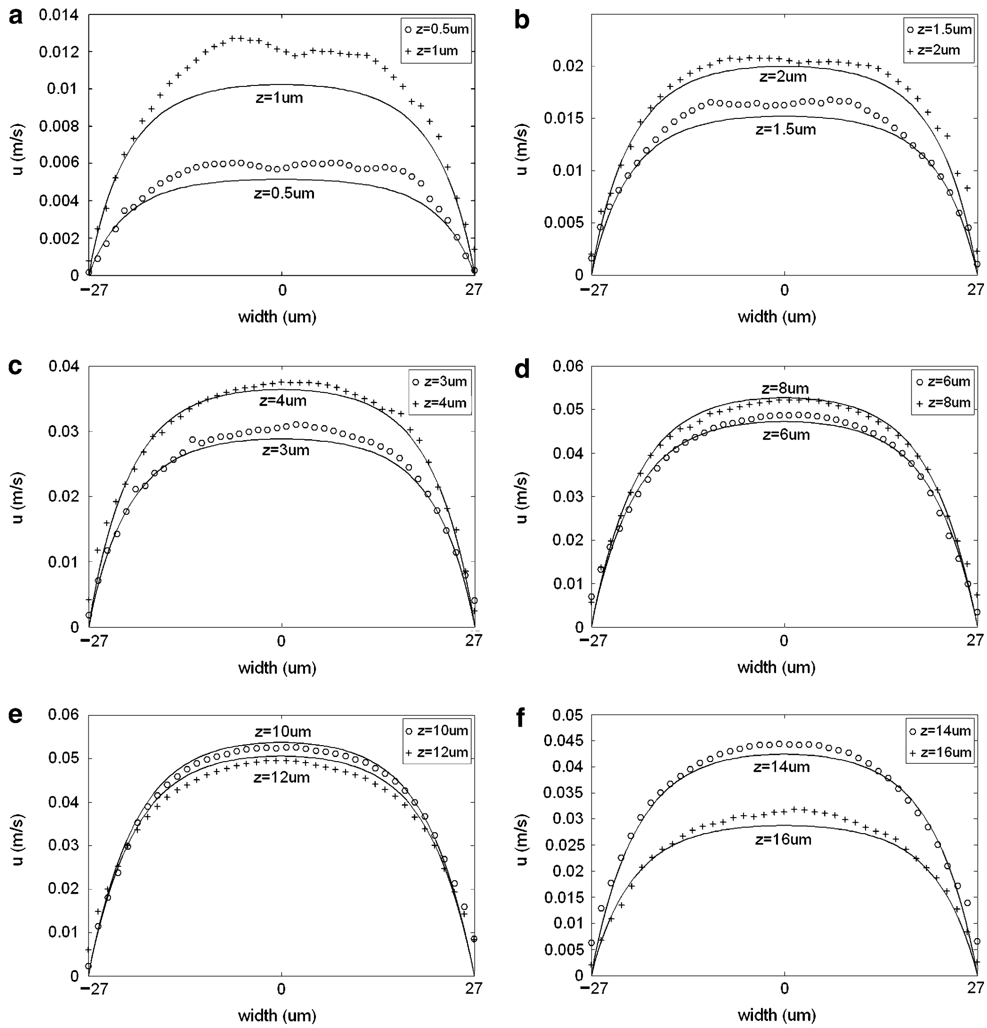

Fig. 7 The comparison of the experimental and theoretical velocities in 12 x–y planes from z = 0.5 to 16 μm, the *circle* and the *plus symbols* are experimental data, the *solid lines* are the theoretical profiles (Re = 1.8)

position (y = 0), the relative deviations ε are 17.4, 18.0, 6.0 and 3.8%, respectively. It is obvious that the relative deviations ε are beyond the range of the error bars in Fig. 7a.

At the position of z = 3–6 μm (z^+ = 0.157–0.314, Fig. 7c, d), the difference between the experimental data and the theoretical values becomes very small. The average relative deviations $\bar{\varepsilon}$ are only 0.8–2.2%, and the relative deviations ε in the center (y = 0) of each x–y plane vary from 1.4 to 3.6%.

In the middle of the channel (z = 8–12 μm, z^+ = 0.421–0.632, Fig. 7d, e), the experimental values are nearly the same as the theoretical ones, with the average relative deviations $\bar{\varepsilon}$ being only 0.2 to −1.0%, and the relative deviations ε in the center of each plane (y = 0) varying from −0.7 to −3.6%.

However, at the positions of z = 14–16 μm (z^+ = 0.737–0.842, Fig. 7f), the experimental velocities become larger than theoretical velocities again, and the average relative deviations $\bar{\varepsilon}$ vary from 2.4 to 5.1%, and the relative deviations ε in the center of each plane (y = 0) vary from 3.1 to 8.5%.

The above experimental results in the horizontal planes show that, the measured velocities were consistent within the experimental error with theoretical velocity when z^+ > 0.05, but large deviations were observed near wall (z^+ < 0.05). The experiments were carried out in another rectangular microchannel at Re = 3.6 and the same trend was observed.

3.2.2 *Velocity profile in* x–o–z *vertical plane*

Considering the geometric symmetry of the rectangular microchannel, we only analyze one velocity profile at the central vertical plane (at y = 0, from z = 0 to 18 μm). The measured velocity data in the center (y = 0) of each horizontal plane are used here (Fig. 8). The error bars in Fig. 8 indicate the standard deviations σ at y = 0 position. It is shown that the experimental values at the center of the

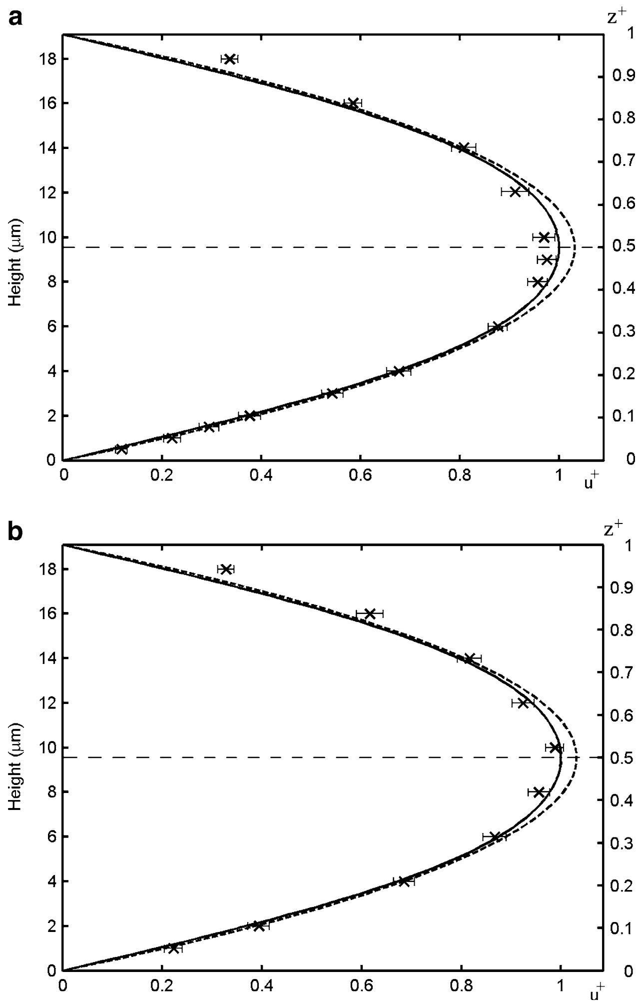

Fig. 8 Velocity profiles in vertical *x–o–z* plane, the *solid lines* in the figure are the theoretical velocity profiles, the *dashed lines* are Poiseuille velocity profile, and the *cross symbols* are the experimental data

x–o–z plane ($z^+ = 0.5$) are slightly smaller than the theoretical values, and the value from a Poiseuille profile are even larger than the theoretical values. The relative deviations ε between experimental data and theoretical results at the points located in the lower half part of the *x–o–z* plane are shown in Table 3.

Table 3 shows that the experimental velocities in the center of the channel are consistent with the theoretical results. At $z^+ = 0.419–0.627$, the deviations between experimental data and theoretical values are below 3.6%. However, between the experimental data and the values calculated from the 2D Poiseuille solution, the discrepancies reach 5%, which implies that 2D profile is no longer a perfect theoretical approximation since $\alpha = 0.35$. In the near wall region ($z^+ \le 0.052$), it is remarkable that the experimental velocities are larger than the theoretical velocities, we will discuss this phenomena in Sect. 4.

We also noted the asymmetry of the experimental date in *x–o–z* plane (Fig. 8). The measured velocities at the upper position (z = 14–18 μm, $z^+ = 0.73–0.94$) are slightly larger than that at the symmetric lower position. Although the rectangular microchannels are geometrically symmetric, the material properties of the upper wall and the substrate are different. The upper wall is made of hydrophobic PDMS, while the glass substrate at the bottom is hydrophilic. This may be the reason resulting in relatively larger experimental velocities at upper position (Degré et al. 2006). Another reason may relate to the limitation of working distance of oil immersed objective of the inverted microscope and the effect of the oil film. A 100×/1.35 oil immersed objective was used in the experiments, and the working distance is only 100 μm. When the focus plane is adjusted toward the upper channel, the change of the oil film thickness may affect the measurement position.

The above experimental results show that the velocity profiles at horizontal *x–y* planes and vertical *x–o–z* plane are consistent with the theoretical profiles, except in the near wall region ($z^+ < 0.05$). The comparison results in *x–o–z* plane indicate that the 2D Poiseuille profile is no longer a perfect theoretical approximation since $\alpha = 0.35$.

4 Discussions

The substrate of the microchannel is hydrophilic glass with CA = 20–30°, so the slip on the substrate can be neglected

Table 3 The relative deviations between experimental data and theoretical values in the vertical *x–o–z* plane ($Re = 1.8$)

Position	0.5 μm $z^+ = 0.026$ (%)	1 μm $z^+ = 0.052$ (%)	2 μm $z^+ = 0.104$ (%)	4 μm $z^+ = 0.209$ (%)	6 μm $z^+ = 0.314$ (%)	8 μm $z^+ = 0.419$ (%)	10 μm $z^+ = 0.523$ (%)	12 μm $z^+ = 0.627$ (%)
ε_{z-T}[a]	+17.4	+18.0	+3.8	+3.0	+2.1	−1.6	−2.4	−3.6
ε_{z-P}[b]	+14.5	+9.8	−1.0	+0.7	−0.6	−4.0	−4.8	−5.0

[a] ε_{z-T}: relative deviation with respect to theoretical profile

[b] ε_{z-P}: relative deviation with respect to Poiseuille profile

here (Cottin-Bizonne et al. 2005; Honig and Ducker 2007). But in the experiment, the measured velocities near wall are obviously larger than no-slip theoretical results. This phenomenon is similar as the "near wall measurement effect" called by Devasenathipathy et al. (2003). They observed that in a rectangular microchannel ($\alpha = 1.07$), the experimental values near the wall were 6% larger than those predicted by 3D theory. Some physical effects which may influence the near wall velocity measurement will be considered:

1. The near wall hydrodynamic resistance. Considering the hindered motion of a sphere particle close to wall, Goldman et al. (1967) discussed the relation between the velocity of particle u_p and the velocity of fluid u_f in a shear flow as:

$$\frac{u_p}{u_f} \approx 1 - \frac{5}{16}\left(\frac{r}{z}\right)^3 \tag{6}$$

where r is the radius of the particle, z is the distance from the center of the particle to the wall. Based on Eq. 6, if $r/z = 0.2$, so $u_p/u_f \approx 0.9975$. It means that the particle velocity is smaller than the local fluid velocity. However, in our experiments, the measured velocities are larger than the theoretical velocities.

2. Wall slip. Many previous studies attributed the larger measured velocity near wall to slip directly (reviewed by Neto et al. 2005; Lauga et al. 2007). According to Navier's (1823) slip model, the slip velocity u_{slip} can be expressed as:

$$u_{slip} = b\frac{\partial u}{\partial y}\Big|_{wall} = b\gamma \tag{7}$$

where b is the slip length, γ is the shear rate at the wall. If we consider the difference between the experimental velocity and the theoretical velocity at $z = 0.5$ μm position to be the slip velocity, i.e. $u_{slip} = u_{exp} - u_{theo}$, based on Figs. 7a and 8a, the u_{slip} can be evaluated as approximately 0.5 mm/s and the shear rate γ is approximately 10^4 s^{-1}. As a result, slip length $b \approx 50$ nm. But hydrophilic walls were used in the experiments, and there should be no slip on hydrophilic walls (Cottin-Bizonne et al. 2005, Honig and Ducker 2007). It is surprising to obtain a relatively large slip length on this wall.

3. Electrophoretic motion of the particles due to streaming potential. Lauga (2004) proposed that one kind of "apparent slip" is in fact the electrophoretic motion of the particles due to streaming potential. Under the assumption that surface potential is low and the thickness of the electric double layer is thin, i.e. $e\zeta_w << k_B T$, $\kappa^{-1} << h$, the electrophoretic velocity u_E of particles can be expressed as:

$$u_E = \frac{\varepsilon_r^2 \varepsilon_0^2 \zeta_w \left(2/3\zeta_p - \zeta_w\right)}{\sigma_c \mu^2}\frac{dp}{dx} \tag{8}$$

where ε_0 is the permittivity of vacuum, ε_r is the relative permittivity, dp/dx is the pressure gradient, μ is the viscosity of the fluid, σ_c is the ionic conductivity, e is electronic charge, ζ_w and ζ_p are the zeta potential on the wall and on the particle surface, respectively. It is hard to measure the wall zeta potential accurately, so we use accepted values (Joseph and Tabeling 2005; Lauga 2004; Lumma et al. 2003) to evaluate u_E. The calculation result is $u_E \approx 0.1$ mm/s, and the slip length $b \approx 10$ nm. Obviously, it is not sufficient to attribute the large apparent slip near wall merely to the electrophoretic motion of the particles.

4. Wall depletion layer. Due to the electrostatic repulsion or the strong shear flow near wall, particles may move away from wall and a depletion layer appears. Lumma et al. (2003) suggested that the thickness of the depletion layer due to interaction between particles and wall was 0.9 μm for pure water. Hartman Kok et al. (2004) observed a submicron thickness wall depletion layer for submicron particles, and suggested the thickness of the depletion layer depended on the Peclet number. But Huang et al. (2006) suggested that the thickness is smaller than 100 nm. In our experiments, although we could not measure the thickness of the depletion layer, we observed the concentration of the particles increased when the measurement position moved from $z = 0.5$ to 1 μm. Considering the Debye length in pure water is approximately 300 nm, it is reasonable that a submicron depletion layer exists due to electrostatic repulsion. The particles may be repulsed a very short distance away from the wall, and therefore have larger velocities. However, more experimental studies are needed to verify the effects of the depletion layer.

As discussed above, there are some important physical effects which may affect the measured velocities at the bottom wall of the channel. Velocity measurements using tracer particles near a wall should be very carefully analyzed. In our case, the wall depletion layer due to electrostatic repulsion may be the main effect lead to the relatively large measured velocity near wall.

5 Conclusions

With the microPIV system and the pressure driven apparatus, we measured the velocity profiles in 14 horizontal planes along z direction of rectangular microchannels with $\alpha = 0.35$ at $Re = 1.8$ and 3.6. The experimental data of velocities in x–y and x–o–z planes are compared with the theoretical values of the fifth order approximation and the Poiseuille's values, respectively. The results show that:

1. For a rectangular microchannel with moderate aspect ratio ($\alpha = 0.35$), the measured velocity profiles in horizontal x–y and vertical x–o–z planes are in agreement with theoretical profiles. The relative deviations ε between experimental data and theoretical values in each horizontal x–y plane are less than 3.6%, except for the planes close to wall at $z^+ \le 0.05$ ($z \le 1$ μm). The horizontal velocity profiles also show 3D behaviors.
2. The deviation of the vertical velocity profile in the x–o–z plane between the experiments and Poiseuille formula reaches to 5%. It implies that Poiseuille profile is suitable as a theoretical approximation only when the aspect ratio $\alpha \le 0.35$ for a rectangular microchannel.
3. The values of measured velocities are relatively large at $z^+ \le 0.05$ ($z \le 1$ μm) on a hydrophilic wall. Some physical effects may influence the near wall measurement when tracer particles are used, including the electrophoretic motion of particles due to streaming potential, the near wall depletion layer and so on. Based on the discussion above, the depletion layer due to electrostatic repulsion is suggested as the main effect. It is worthwhile to make further study of this phenomenon.

Acknowledgments The authors gratefully acknowledge the support of this work by the Major Innovation Project of Chinese Academy of Sciences (KJCX2-SW-L2) and National Natural Science Foundation of China (10672172).

References

Boussinesq J (1868) Memoire sur l'influence des frottements dans les mouvements reguliers des fluids. J Math Pures Appl Deuxieme Ser 13:377–424

Cottin-Bizonne C, Cross B, Steinberger A, Charlaix E (2005) Boundary slip on smooth hydrophobic surfaces: intrinsic effects and possible artifacts. Phys Rev Lett 94:056102

Degré G, Joseph P, Tabeling P, Lerouge S, Cloitre M, Ajdan A (2006) Rheology of complex fluids by particle image velocimetry in microchannels. Appl Phys Lett 89:024104

Devasenathipathy S, Santiago JG, Wereley ST, Meinhart CD, Takehara K (2003) Particle imaging techniques for microfabricated fluidic systems. Exp Fluids 34:504–514

Goldman AJ, Cox RG, Brenner H (1967) Slow viscous motion of a sphere parallel to a plane wall—ii: Couette flow. Chem Eng Sci 22:653–660

Gui L, Wereley ST, Lee SY (2002) Digital filters for reducing background noise in microPIV measurements. In: Proceedings of the 11th international symposium on the application of laser techniques to fluid mechanics, Lisbon

Hartman Kok PJA, Kazarian SG, Briscoe BJ, Lawrence CJ (2004) Effects of particle size on near-wall depletion in mono-dispersed colloidal suspensions. J Colloid Interface Sci 280:511–517

Honig CDF, Ducker WA (2007) No-slip hydrodynamic boundary condition for hydrophilic particles. Phys Rev Lett 98:028305

Huang P, Guasto JF, Breuer K (2006) Direct measurement of slip velocities using three-dimensional total internal reflection velocimetry. J Fluid Mech 566:447–464

Joseph P, Tabeling P (2005) Direct measurement of the apparent slip length. Phys Rev E 71:035303

Lauga E (2004) Apparent slip due to the motion of suspended particles in flows of electrolyte solutions. Langmuir 20:8924–8930

Lauga E, Brenner MP, Stone HA (2007) Microfluidics: the no-slip boundary condition. In: Handbook of experimental fluid dynamics. Springer, Berlin

Lauga E, Squires TM (2005) Brownian motion near a partial-slip boundary: a local probe of the no-slip condition. Phys Fluids 17:103102

Li H, Olsen MG (2006) MicroPIV measurements of turbulent flow in square microchannels with hydraulic diameters from 200 μm to 640 μm. Int J Heat Fluid Flow 27(1):123–134

Lumma D, Best A, Gansen A, Feuilebois F, Radler JO, Vinogradova OI (2003) Flow profile near a wall measured by double focus fluorescence cross-section. Phys Rev E 67:056313

Meinhart CD, Wereley ST, Santiago JG (1999) PIV measurements of a microchannel flow. Exp Fluids 25:414–419

Navier CLMH (1823) Mémoire sur les lois du mouvement des fluids Mem. Acad Sci Inst Fr 6:389–416

Neto C, Evans DR, Bonaccurso E, Butt H-J, Craig V (2005) Boundary slip in Newtonian liquids: a review of experimental studies. Rep Prog Phys 68:2859–2897

Olsen MG, Adrian RJ (2000) Out-of-focus effects on particle image visibility and correlation in microscopic particle image velocimetry. Exp Fluids 29(7):S166–S174

Ou J, Rothstein JP (2005) Direct velocity measurements of the flow past drag-reducting ultrahydrophobic surfaces. Phys Fluids 17:103606

Patel VC, Head MR (1969) Some observations on skin friction and velocity profiles in fully developed pipe and channel flows. J Fluid Mech 38:181–201

Santiago JG, Wereley ST, Meinhart CD, Beebe DJ, Adrian RJ (1998) A partical image velocimetry system for microfluidics. Exp Fluids 25:316–319

Schlichting H (1979) Boundary layer theory, 7th edn. McGraw-Hill Book Company, New York, pp 612–615

Silber-Li ZH, Tan YP, Weng PF (2004) A microtube viscometer with a thermostat. Exp Fluids 36(4):586–592

Stone HA, Strook AD, Ajdari A (2004) Engineering flows in small devices: microfluidics toward a Lab-on-Chip. Annu Rev Fluid Mech 36:381–411

Tretheway DC, Meinhart CD (2002) Apparent fluid slip at hydrophobic microchannel wall. Phys Fluids 14(3):L9–L11

White FM (1974) Viscous fluid flow. McGraw-Hill Book Company, New York, pp 123